



Structural, magnetic, optical and electronic properties of Gd_2NiIrO_6

G. Bhavani^a, T. Durga Rao^{a,*}, Manish K. Niranjan^b, K. Ramesh Kumar^a, B. Sattibabu^a, V. Petkov^c, E.S. Kannan^d, B.H. Reddy^e

^a Department of Physics, GITAM (Deemed to Be University), Visakhapatnam, Andhra Pradesh, 530045, India

^b Department of Physics, Indian Institute of Technology Hyderabad, Telangana, 502284, India

^c Department of Physics, Central Michigan University, Mt. Pleasant, MI, 48858, USA

^d Department of Physics, K K Birla Goa Campus, Zuarinagar, Goa, 403 726, India

^e Department of Physics, Government College (Autonomous), Rajamahendravaram, Andhra Pradesh, 533103, India

ARTICLE INFO

Keywords:

Double perovskite
X-ray diffraction
Weak ferromagnetism
Exchange bias
Optical band gap
Electronic structural studies

ABSTRACT

Polycrystalline Gd_2NiIrO_6 double perovskite compound was synthesized by the solid-state route. Rietveld refinement of the X-ray diffraction pattern revealed that the compound was crystallized in a monoclinic structure with $P2_1/n$ space group (IUCr. No. 14). The scanning electron micrograph showed that the grains were spherical and well distributed with an average grain size of around 1 μm . The temperature-dependent magnetic measurements showed magnetic transitions at 165 K and 149 K in the low-temperature region. Below the transition temperatures, weak ferromagnetism was evidenced by field-dependent magnetization measurements. Exchange bias effects were observed which were driven by Dzyaloshinsky–Moriya interactions in the compound. The UV–visible measurement evidenced that the compound had an optical band gap of 1.8 eV. The electronic structure calculations using the DFT + U method revealed that Gd_2NiIrO_6 compound exhibited a bandgap only when on-site correlations for the d -states were included, and the calculation showed that the AF1 configuration was energetically favourable.

1. Introduction

Double perovskite oxides with the general formula $A_2BB'O_6$ ($A = Sr, Ca, Pb, La, Nd, Gd, etc.$, and B/B' is a transition metal ion) have been studied extensively since the 1950s [1]. These materials have garnered significant attention due to their ability to incorporate diverse elements at the B and B' sites, as well as their interesting physical properties, such as high Curie temperature, colossal magnetoresistance, metal-insulator transition, etc. [2–5]. The physical properties of these materials mainly depend on the chemical structure, nature and the oxidation states of transition metal ions. The double perovskites with 5d transition metal elements at the B/B' site would offer fascinating properties compared to those systems with 3d metal elements at both the B and B' sites. The 5d iridium-based oxide double perovskites show exotic properties such as Weyl semimetals, Kitaev spin liquid, novel Mott insulator [6], etc., due to the strong spin-orbit coupling (SOC) with an energy comparable to on-site Coulomb interaction and crystal field energies [7]. The Ir and Ni-based double perovskite compounds were synthesized in 1965 [8], and their magnetic properties were investigated

in 1993 [9]. Recently, T. Ferreira et al. synthesized a series of Ir-based double perovskites with the chemical formula $R_2TlR'O_6$ ($R = La, Pr, Nd, Sm-Gd; T = Mg, Ni$) and investigated their structural and magnetic properties. For smaller A-site lanthanide cations, larger monoclinic distortions and smaller Ni–O–Ir bond angles are observed in the unit cell, which leads to higher magnetic ordering temperatures [10]. The magnetic ground state and electronic properties of the La_2NiIrO_6 compound have also been explored [11,12], and its exchange bias (EB) properties are extensively studied [13]. Exchange bias (EB) manifests off-centering of magnetic hysteresis loops along the axes [14]. When a system consisting of ferromagnetic (FM) and antiferromagnetic (AFM) spin interface is cooled below the Néel temperature (T_N) of the AFM material in an external magnetic field, anisotropy (exchange bias) is induced at the interface, leading to the shift of hysteresis loops. The EB effects have been studied extensively in diverse systems like FM films on AFM single crystals [15], nanoparticles [16], intermetallics [17], bulk compounds such as Cobaltites, Manganites and in other perovskite compounds [18–20]. However, it is reported that low crystallographic symmetry La_2NiIrO_6 compound exhibited EB properties due to

* Corresponding author.

E-mail address: dtadiset@gitam.edu (T. Durga Rao).

<https://doi.org/10.1016/j.physb.2024.416477>

Received 4 July 2024; Received in revised form 25 August 2024; Accepted 29 August 2024

Available online 31 August 2024

0921-4526/© 2024 Elsevier B.V. All rights are reserved, including those for text and data mining, AI training, and similar technologies.

Dzyaloshinsky-Moria (D-M) interactions [13]. The Hamiltonian for the interaction between spins is given as

$$H = \sum_{\langle ij \rangle} \left[J_{ij} \vec{S}_i \cdot \vec{S}_j + \vec{D}_{ij} \cdot (\vec{S}_i \times \vec{S}_j) \right] \quad 1$$

where J_{ij} is the exchange interaction between the spins S_i and S_j . The second term in equation (1) is due to the D-M interaction, which favours the canting of spins and produces weak ferromagnetism in the antiferromagnetic structure.

As the $\text{Gd}_2\text{NiIrO}_6$ compound is isostructural to the $\text{La}_2\text{NiIrO}_6$ compound, it can be expected that the $\text{Gd}_2\text{NiIrO}_6$ compound will show exchange bias properties due to D-M interactions. The exploration of exchange bias effects in the double perovskite oxides may offer an additional degree of freedom in device applications, such as permanent magnets, spintronics, magnetic recording media, etc, along with interesting physics. To the best of our knowledge, the structural and magnetic properties of the $\text{Gd}_2\text{NiIrO}_6$ compound have been reported so far, leaving a significant gap in the literature regarding its other properties, such as optical, electronic, dielectric, etc. A comprehensive investigation into these aspects is essential, as it would not only deepen our understanding of the intrinsic properties of the $\text{Gd}_2\text{NiIrO}_6$ compound but also provide valuable insights for potential device applications. Based on the above discussion, we have synthesized the $\text{Gd}_2\text{NiIrO}_6$ compound by solid-state reaction and carried out its structural, magnetic, optical and electronic structural calculation studies.

2. Experimental details

Polycrystalline $\text{Gd}_2\text{NiIrO}_6$ (GNIO) double perovskite compound was prepared by the solid-state route. Stoichiometric amounts of Gd_2O_3 , NiO and IrO_2 metal powders were mixed and ground for 3 h thoroughly. The powder was calcined at 1000°C for 24 h, then at 1100°C for 24 h and finally at 1200°C for 24 h. The calcined powder was made as a pellet and sintered at 1220°C for 24 h. The crystal structure of the compound was confirmed by X-ray diffractometer (Bruker D8-Discover diffractometer with $\text{Cu K}\alpha$ radiation). The scanning electron microscope (MIRA 3 LMU, Tescan, Brno, Czech Republic) equipped with energy dispersive x-ray spectroscopy was used to study the microstructure of the compound. Magnetic properties were investigated using a physical property measurement system (PPMS) with a VSM assembly (Quantum Design, USA). The optical energy band gap studies were conducted on a UV-VIS-NIR spectrometer (SHIMADZU) in the absorbance mode.

The ab-initio quantum mechanical calculations are performed using the plane wave basis set formalism within the framework of density functional theory (DFT) [21] as implemented in the VASP Package [22]. The interactions between core and valence electrons are approximated using the projected augmented wave (PAW) potentials [23]. The GGA + U approach [24] is used to include the on-site correlations for the d orbitals on atoms. In the case of Gd atoms, the localised $4f$ states and semi-core $3p$ states are treated as core states and valence states, respectively. The $(5d^7, 6s^2)$, $(3d^8, 4s^2)$, $(2s^2, 2p^4)$ valence electron configurations are considered for Ir, Ni, and O atoms, respectively. The exchange-correlation (XC) effects are treated using the Perdew-Burke-Ernzerhoff (PBE) [25] form of generalized gradient approximation (GGA). A kinetic energy cutoff of a minimum of 520 eV is used to expand the Kohn-Sham orbitals in a plane wave basis set. The integrations in the k -space are performed by sampling the Brillouin zone using $8 \times 8 \times 6$ Monkhorst-Pack k -point mesh. The lattice parameters and the fractional coordinates of the atoms in the unit cell are relaxed until the Hellmann-Feynman forces become less than $10 \text{ meV}/\text{\AA}$. Self-consistency in calculations is achieved with total energies converging down to 10^{-6} eV/cell .

3. Results and discussions

3.1. Structural and microstructure studies

The X-ray diffraction (XRD) pattern of the polycrystalline GNIO compound at room temperature is shown in Fig. 1. Inset in the figure shows the crystal structure of the GNIO compound. The crystal structure of the GNIO compound is analyzed by Rietveld refinement using Fullprof software [26]. From the refinement, it is observed that the compound crystallizes in a monoclinic structure with $P2_1/n$ space group (*IUCr* No. 14). The obtained lattice parameters, position coordinates and site occupancies from the refinement are given in Table 1. The appearance of (011) and (013) superstructure reflections in the XRD pattern at around 19.37° and 38.4° respectively, indicates the presence of rock-salt ordered arrangements of Ni and Ir cations in BO_6 and $\text{B}'\text{O}_6$ octahedra as is observed in some $\text{A}_2\text{BB}'\text{O}_6$ double perovskites [13,27,28]. Although there exists a long-range ordering of B and B'-site cations, the anti-site disorder is quite common in these compounds. In $\text{A}_2\text{BB}'\text{O}_6$ double perovskites, the disordered arrangement of B-site ions is referred to as anti-site disorder (ASD). ASD results in B-O-B', B-O-B, and B'-O-B' interactions, which can significantly alter the magnetic and other intrinsic properties of these materials. For instance, D. Rubi et al., observed an increase in the Curie temperature of $(\text{Ca}_{1-x}\text{Nd}_x)_2\text{Fe}_{1+x}\text{Mo}_{1-x}\text{O}_6$ materials for $x > 0$, attributing this enhancement to the presence of disorder [29]. Similarly, in the $\text{Sr}_2\text{FeMoO}_6$ double perovskite, studies on cationic Fe/Mo ordering have demonstrated that cation disorder influences the material's saturation magnetization [30]. More broadly, disorder plays a crucial role in determining the magnetic, optical, thermal, and electrical properties of materials. The B-site (Ni/Ir) cation degree of order can be estimated as $S = 2g_B - 1$, where g_B is the occupancy of the B-site cation on its correct site [31]. For complete ordering of B-site, $S = 1$, whereas for complete disorder, $S = 0$. Relatively, better fitting is observed in the XRD pattern after allowing the B-site cation disorder in their sites. The value of S is found to be 0.976, indicating a small amount of B-site cation disorder present in the compound. The refined composition of the compound can be modelled as $\text{Gd}_2[\text{Ni}_{0.4940}\text{Ir}_{0.0060}]_2\text{b}[\text{Ir}_{0.4942}\text{Ni}_{0.0058}]_2\text{aO}_6$ [32,33].

The crystal structure of double perovskites can be analyzed using the Goldschmidt tolerance factor t , which defined as

$$t = \frac{1}{\sqrt{2}} \left[\frac{r_A + r_O}{\left(\frac{r_B + r_{B'}}{2} \right) + r_O} \right] \quad 2$$

where r_A , r_B , $r_{B'}$ and r_O , are radii of ions at their respective sites. For $1.05 > t > 1$, the crystal structure adopts cubic with $Fm\bar{3}m$ structure; for $1 > t > 0.97$, it adopts tetragonal; and for $0.97 > t$, it adopts orthorhombic or monoclinic [34]. The calculated value of t obtained using equation (2) is 0.8604, which is also in corroboration with the stabilization of the monoclinic crystal structure of GNIO.

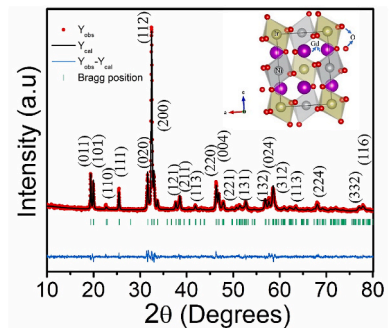


Fig. 1. Room temperature XRD pattern of GNIO compound. The inset shows the crystal structure of GNIO.

Table 1

Lattice parameters, position coordinates, site occupancies and reliability factor of $\text{Gd}_2\text{NiIrO}_6$ in the monoclinic structure with $P2_1/n$ space group, at 300 K. Gd, O1, O2 and O3 atoms at $4e$ (x, y, z) sites, Ni at $2b$ ($0,0,1/2$), Ir at $2a$ ($0,0,0$).

| | |
|------------------------------------|---------------|
| a Å | 5.4284(5) |
| b Å | 5.6546(6) |
| c Å | 7.7497(8) |
| V Å ³ | 237.88 |
| β (°) | 90.118(8) |
| Gd | |
| x | 0.0235 |
| y | 0.5587 |
| z | 0.7500 |
| Occupancy | 0.9940 |
| (Ni/Ir) _{2b} | |
| Occupancy (Ni/Ir) _{2b} | 0.4940/0.0060 |
| (Ir/Ni) _{2a} | |
| Occupancy (Ir/Ni) _{2a} | 0.4942/0.0058 |
| O1 | |
| x | 0.1677 |
| y | 0.0600 |
| z | 0.2288 |
| Occupancy | 1.0428 |
| O2 | |
| x | 0.2168 |
| y | 0.2497 |
| z | -0.036 |
| Occupancy | 0.9975 |
| O3 | |
| x | 0.2311 |
| y | 0.2954 |
| z | 0.5596 |
| Occupancy | 1.0764 |
| Overall B-factor (Å ²) | 0.6 |
| Reliability factor | |
| χ^2 | 1.60 |

Fig. 2 shows the microstructure image of the GNIO compound. It is evident that the compound has homogeneous, identical and spherical grains with an average grain size of around 1 μm . The compound has some pores, indicating its density is lower. The atomic percentages of constituent elements as obtained from energy-dispersive X-ray (EDAX) analysis indicate that the compound maintains stoichiometry in the ratio Gd:Ni:Ir:O close to 2:1:1:6, which is in corroboration with the X-ray findings.

3.2. Magnetic studies

The zero-field cooled (ZFC) and field-cooled (FC) magnetization of the GNIO compound, measured from 5 K to 300 K under 1 kOe, is shown in Fig. 3 (a). The ZFC and FC curves merge with each other from 300 K to 160 K, below which the two curves start bifurcating. The ZFC curve increases with the decrease in temperature until 85 K, below which the magnetization decreases up to 15 K. Again the magnetization starts increasing from 15 K to 5 K with the further decrease in temperature.

In contrast, the FC magnetization shows an increasing trend as the temperature decreases. Notably, two magnetic transitions are detected at 165 K and 149 K. These transitions are also evident in the first derivative of the ZFC curve, as shown in the inset of Fig. 3 (a). In the case of a single crystal, the magnetic transition is observed at 170 K [10]. Fig. 3 (b) shows the magnetization hysteresis plots of the GNIO compound measured at temperatures 5 K and 300 K. The M - H curve measured at 300 K shows the paramagnetic nature, whereas the M - H loop measured at 5 K shows a remanent magnetization (M_r) of 0.09 emu/g and a coercive field (H_c) of 575 Oe. The non-saturation of magnetization curves with the field (up to the maximum applied field) indicates the presence of an antiferromagnetic nature of the compound. Further, a non-zero remanent magnetization in the low temperature has appeared in the M - H loop, as shown in the inset of Fig. 3 (b), with the enlarged view of the M - H curve near the origin. A nonzero remanent magnetization is attributed to the presence of weak ferromagnetism (WFM) in the compound due to Dzyaloshinsky–Moriya (D-M) interactions [35]. The hysteresis loops centered at the zero field are observed, indicating no exchange bias properties in the M - H curve under zero field cooled conditions. To test the exchange bias properties in the GNIO sample, a field-cooled (FC) M - H hysteresis loop under a cooling field 8T is measured between ± 70 kOe at 10 K, 20 K, and 150 K as shown in Fig. 4. It is observed that FC M - H hysteresis loops show a shift in the magnetic field axis, indicating the presence of exchange bias properties in the compound.

The exchange bias field H_E , and remanence asymmetry M_E are defined as $H_E = -\frac{H_1+H_2}{2}$, and $M_E = -\frac{M_{R_1}+M_{R_2}}{2}$ respectively, where H_1 and H_2 are respectively the left and right coercive fields, M_{R_1} and M_{R_2} are respectively the positive and negative remanent magnetizations. The magnitude of values of H_E and M_E are calculated and given in Table 2. Generally, the EB effects are observed due to the development of exchange interactions between the WFM and AFM interfaces. The WFM could be due to the canting of antiferromagnetic spins in the compound. The canting of spins arises due to D-M interactions and/or due to the

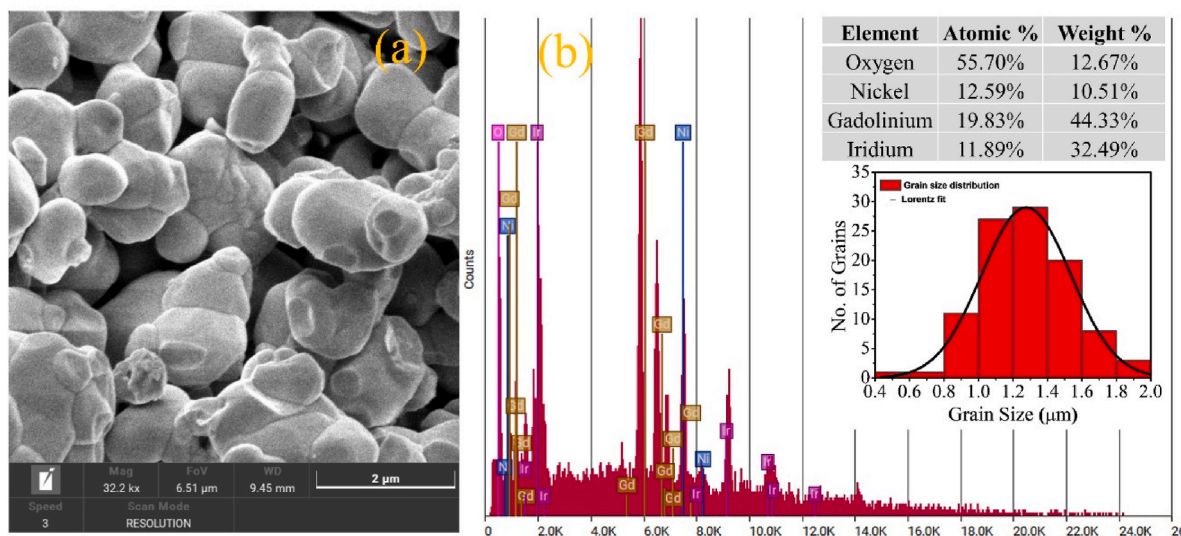


Fig. 2. (a) SEM micrograph and, (b) Energy dispersive spectroscopy (EDS) spectrum of GNIO compound.

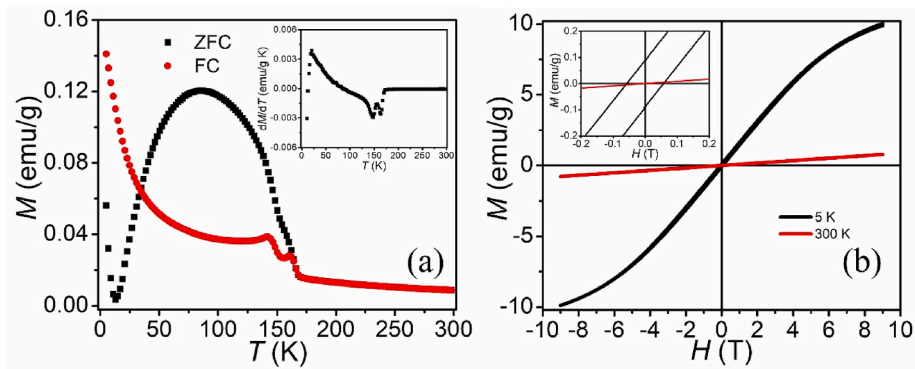


Fig. 3. (a) ZFC-FC magnetization curves of GNIO compound measured under 1 kOe. Inset in (a) shows the derivation of magnetization, (b) M - H loops of GNIO compound at 5 K and 300 K and Inset shows the enlarged view of the same M - H plot.

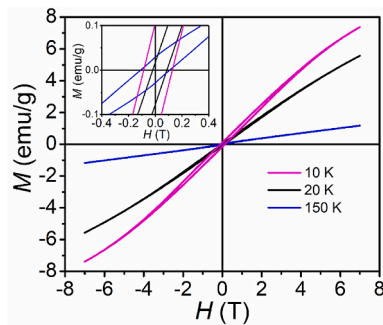


Fig. 4. FC M - H curves of GNIO compounds at 10 K, 20 K and 150 K. Inset shows an enlarged view of M - H curves near the origin.

Table 2

The variation of H_E and M_E of GNIO compound at different temperatures.

| Temperature (K) | H_E (Oe) | M_E (emu/g) |
|-----------------|------------|---------------|
| 10 | 210 | 0.0267 |
| 20 | 343.5 | 0.007 |
| 150 | 8 | ~ 0 |

anisotropy of the compound. The increase in irreversibility between ZFC and FC curves signifies the increase in WFM below 165 K due to D-M interactions and/or to the anisotropy of the compound. It is reported that the low crystallographic symmetric compounds such as $\text{La}_2\text{BiIrO}_6$ ($B = \text{Cu/Zn}$), along with the strong spin-orbit coupling, facilitate D-M interactions [36,37]. These D-M interactions would have caused WFM in the AFM matrix of the $\text{Gd}_2\text{NiIrO}_6$ compound and led to the observed exchange bias properties. In some perovskite compounds with AFM structures, the EB effects are observed because of D-M interactions [38, 39]. In the GNIO compound, the EB effects could be ascribed to the development of exchange interactions between the WFM components and the AFM matrix. During the FC process, the freezing of these uncompensated spins will induce the exchange anisotropy and hence, the exchange bias in the compound. At low temperatures (10 K and 20 K), the irreversibility between ZFC and FC curves is high, and a strong WFM component is expected, and hence higher exchange interactions between the WFM components and the AFM matrix. Hence, the EB effects are significant. At 150 K, the irreversibility is very small, and the EB effects weaken, implying a decrease in exchange contacts. The appearance of remanence asymmetry M_E is due to the presence of uncompensated pinned spins in the AFM material [40], and the exchange bias field H_E is due to exchange interaction between the AFM/FM interfaces [41].

3.3. UV-visible spectroscopy

The optical properties of the compound are studied by analyzing its UV-vis absorption spectrum. Fig. 5 shows the absorption spectrum of the GNIO compound. The optical band gap of the GNIO compound is calculated using Tauc's equation [42].

$$(\alpha h\nu)^n = A(h\nu - E_g) \quad 3$$

where α , A , $h\nu$, and E_g are the coefficient of absorption, proportional constant, photon energy, and energy gap respectively.

Inset of Fig. 5 shows a plot drawn between $(\alpha h\nu)^2$ and $h\nu$. The intercept of the tangent drawn to the most linear portion of the curve gives the band gap E_g which is found to be 1.8 eV. From the obtained band gap, the sample is classified as a semiconductor [43]. J. A. Khan et al. observed an indirect band gap of 0.96 eV in the $\text{La}_2\text{CrMnO}_6$ sample [44]. S. R. Mohapatra et al. prepared a $\text{Gd}_2\text{NiMnO}_6$ compound by conventional solid-state reaction route and reported a band gap of 1.48 eV in it [45]. The band gap of material has many applications. The wavelength of emitted radiation from LED or Laser diodes strongly depends on the band gap of a material. Researchers have focused on designing materials with desired band gaps to achieve specific applications. The band gap of 1.8 eV in the GNIO compound would be useful in photocatalysis, optoelectronics, solar cells and sensors. Though there have been halide and chalcogenide perovskites which show interesting optical properties in optoelectronics [46,47], the double perovskite oxides offer advantages in terms of chemical and thermal stability, environmental safety, better mechanical properties, and a broader range of functionalities.

3.4. Electronic structure

The spin-polarized calculations are performed using the DFT + U

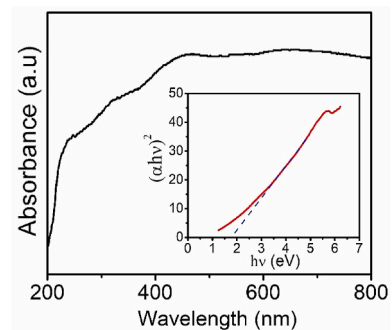


Fig. 5. UV-vis spectrum of GNIO compound. Inset shows the Tauc's plot of GNIO compound.

method to explore the atomic and electronic structure of GNIO. Though we have also performed calculations with the GGA scheme, our results suggest that the bandgap is opened only when on-site correlations and repulsions for the d -states of atoms are considered using the GGA + U scheme. Standard GGA functionals often underperform in describing materials with strongly correlated d or f electrons. The DFT + U method addresses this limitation, providing a more accurate description of these systems. DFT + U can be considered as an approximate spectral-potential method, with U being determined by imposing the piecewise linearity of the total energy with respect to electronic occupations in the Hubbard subspace or manifold. This results in the removal of self-interaction errors, thereby improving the bandgap [48]. We use a value of $U = 3$ eV for all d -orbitals. The calculations are performed for two different anti-ferromagnetic (AF1 and AF2) as well as ferromagnetic (FM) configurations for Ni and Ir atoms. In the AF1 configuration, the Ni magnetic moments are aligned parallel to each other in the (001) plane. Likewise, the Ir magnetic moments are aligned parallel to each other. However, the magnetic moments of Ni are aligned antiparallel to those of Ir. In the case of AF2 configuration, the magnetic moments of both Ni and Ir are aligned antiparallel to each other. The energies of all three configurations are found to be comparable. Our calculations reveal that the AF1 state is energetically favorable, with an energy of 1.1 meV/atom lower than the AF2 state and 3.6 meV/atom lower than the FM state. The observed small energy differences between the AF1, AF2, and FM states suggest a possible competition between various magnetic ordering configurations. This competition could lead to a more complex spin structure or magnetic ordering in the ground state. Furthermore, nano-regions with a different type of AF ordering and/or competing magnetic spin structures may also exist in the system [49]. Table 3 presents the lattice parameters of the optimized unit cell for the AF1, AF2, and FM states. These values were obtained from spin-polarized calculations employing a U value of 3 eV for the d -orbitals of the atoms. The calculated lattice parameters exhibit good agreement with experimental data and align with the expected trends for the GGA exchange-correlation approximation. In general, the GGA approximation slightly overestimates the lattice parameters [50], and the same trend is observed for the GNIO. In the past, using GGA and GGA + U formulations within the full potential linearized augmented plane wave (FP-LAPW) method, theoretical studies on R_2NiMnO_6 ($R = La$ and Gd) have been conducted and the results were reported in Ref. [51]. Using this method, the band gap values of Gd_2NiMnO_6 and La_2NiMnO_6 compounds were found to be 1.36 eV and 1.41 eV, respectively. Table 3 shows that the GGA lattice parameters are slightly overestimated (by < 3 %).

Our GGA calculations yielded a band gap of approximately 1.05 eV, which underestimates the experimental value of ~ 1.8 eV. This underestimation is consistent with the known limitations of the GGA scheme, which can systematically underestimate band gaps by up to 50 % [50]. The absolute value of the magnetic moment of each Ni and Ir atom is found to be $\sim 1.67 \mu_B$ and $\sim 0.75 \mu_B$, respectively. Fig. 6 (a) shows the total and partial density of states (DOS) for GNIO in AF2 configuration. The total DOS of GNIO in AF1, AF2 and FM configurations are shown in Fig. 6 (b). The energy scale in Fig. 6 is rescaled so that the valence band maximum (VBM) is at 0. The valence band (VB) width is ~ 7 eV, with VB extending from ~ -7 eV to VBM at 0 eV.

The states in the VB in range -1.5 eV < E < 0 are mainly comprised

Table 3
Computed lattices parameters and bandgap (eV) of GNIO obtained using GGA + U XC functional scheme.

| | | | a(Å) | b(Å) | c(Å) | V(Å ³) | E _g (eV) |
|------|-----|-----|--------|--------|--------|--------------------|---------------------|
| Cal. | AF1 | GGA | 5.341 | 5.805 | 7.617 | 236.24 | 0.98 |
| | AF2 | GGA | 5.340 | 5.809 | 7.612 | 236.16 | 1.04 |
| | FM | GGA | 5.327 | 5.830 | 7.599 | 236.05 | 1.06 |
| Exp. | – | – | 5.4284 | 5.6546 | 7.7497 | 237.88 | ~ 1.8 |

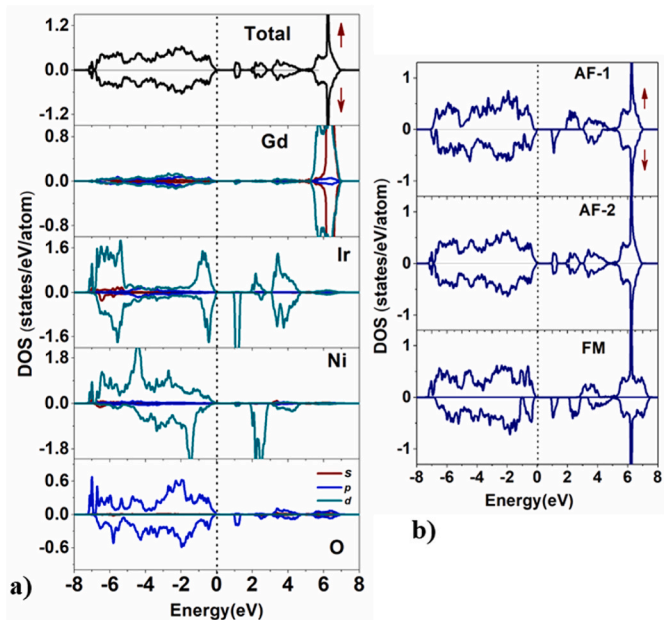


Fig. 6. a) Total and projected density of states for GNIO in AF-2 state. b) Total DOS for GNIO in AF-1, AF-2 and FM states. The dotted line in the DOS plot indicates the valence band maximum.

of Ni-3d, Ir-5d and O-2p states. In the range -1.5 eV < E < -5 eV, the contribution comes primarily from Ni-3d, and O-2p states. The VB in range -5 eV < E < -2 eV are primarily contributed by Ni-3d, and O-2p states. The conduction band (CB) in range 1 eV < E < 4 eV is primarily contributed by Ni-3d, and Ir-5d states. The states in CB in range 5 eV < E < 7 eV are mainly Gd-5d and Gd-5s states. Our theoretical calculation based on DFT using GGA + U scheme predicted an optical band gap of about 0.98–1.0 eV. Fig. 6 (b) shows the DOS for AF1, AF2 and FM configurations, wherein the slight differences between spin-up and spin-down DOS can be clearly seen. In particular, exchange splitting for FM configuration can be seen. Our experimental findings comply qualitatively with theoretically predicted results. As the band gap of the GNIO sample is in the visible region, it can be useful in photocatalysis-based devices.

3.5. Conclusions

Polycrystalline Gd_2NiIrO_6 double perovskite compound was synthesized by solid-state route. Structural analysis using X-Ray diffraction studies indicated that the compound crystallized in a monoclinic structure with $P2_1/n$ space group. The B-site cations showed a nominal amount of disorder at the B-site. Spherical and well-distributed grains were observed from the scanning electron micrographs. Weak ferromagnetism was observed in the low temperature (below 165 K) due to the Dzyaloshinsky-Moriya interactions. The WFM component below the transition temperature, coupled with the antiferromagnetic nature of the compound, led to uncompensated spins in the AFM material, which resulted in the EB properties in the system. The UV-visible spectroscopy studies indicated that the optical band gap of the GNIO sample was 1.8 eV. The electronic structure calculation using the DFT + U method revealed that on-site correlations for the d -states were responsible for the bandgap in Gd_2NiIrO_6 and our calculation showed that the AF1 configuration was energetically favourable.

CRedit authorship contribution statement

G. Bhavani: Writing – original draft, Software, Investigation, Conceptualization. **T. Durga Rao:** Writing – review & editing,

Methodology, Conceptualization. **Manish K. Niranjana**: Software, Formal analysis, Data curation. **K. Ramesh Kumar**: Software, Methodology, Formal analysis, Data curation. **B. Sattibabu**: Software, Formal analysis, Data curation. **V. Petkov**: Software, Formal analysis, Data curation. **E.S. Kannan**: Software, Formal analysis, Data curation. **B.H. Reddy**: Software, Formal analysis, Data curation.

Declaration of competing interest

The authors declare that they have no known competing financial interests or personal relationships that could have appeared to influence the work reported in this paper.

Data availability

Data will be made available on request.

Acknowledgement

Author TDR gratefully acknowledges the financial support provided by UGC-DAE CSR, Mumbai Centre, India through the collaborative research scheme (CRS-M-313) and GITAM RSG project (File No. 2021/0070), Visakhapatnam, India, to carry out this work. Also, this work was supported in part by the U.S. Department of Energy, Office of Basic Energy Sciences under Awards No. DE-SC0021973.

References

- [1] M.T. Anderson, K.B. Greenwood, G.A. Taylor, K.R. Poeppelmeier, *Prog. Solid State Chem.* 22 (1993) 197–233.
- [2] H. Kato, T. Okuda, Y. Okimoto, Y. Tomioka, K. Oikawa, T. Kamiyama, Y. Tokura, *Phys. Rev. B* 65 (2002) 144404.
- [3] K.-I. Kobayashi, T. Kimura, H. Sawada, K. Terakura, Y. Tokura, *Nat. (London)* 395 (1998) 357.
- [4] Y. Krockenberger, K. Mogare, M. Reehuis, M. Tovar, M. Jansen, G. Vaitheeswaran, V. Kanchana, F. Bultmark, A. Delin, F. Wilhelm, A. Rogalev, A. Winkler, L. Alff, *Phys. Rev. B* 75 (2007) 020404.
- [5] M. Azuma, K. Takata, T. Saito, S. Ishiwata, *J. Am. Chem. Soc.* 127 (2005) 8889–8892.
- [6] Y. Gao, Z. Tian, L. Xu, M. Ashtar, Z. Wan, Z. Xia, F. Yang, S. Yuan, Y. Han, W. Tong, *J. Phys. Condens. Matter* 32 (2020) 465802.
- [7] B.J. Kim, H. Ohsumi, T. Komatsu, S. Sakai, T. Morita, H. Takagi, T. Arima, *Science* 323 (2009) 1329.
- [8] G. Blasse, *J. Inorg. Nucl. Chem.* 27 (1965) 993.
- [9] A.V. Powell, J.G. Gore, P.D. Battle, *J. Alloys Compd.* 201 (1993) 73.
- [10] T. Ferreira, G. Morrison, J. Yeon, H. C zur Loye, *Cryst. Growth Des.* 16 (2016) 2795–2803.
- [11] S. Sharma, C. Ritter, D.T. Adroja, G.B. Stenning, A. Sundaresan, S. Langridge, *Phys. Rev. Mater.* 6 (2022) 014407.
- [12] J. Wang, K. Li, B. Yu, Z. Wu, *Comput. Mater. Sci.* 60 (2012) 149–152.
- [13] T. Durga Rao, S. Marik, D. Singh, R.P. Singh, *J. Alloys Compounds*, vol. 705, 2017, pp. 849–852.
- [14] J. Nogues, I.K. Schuller, *J. Magn. Magn. Mater.* 192 (1999) 203.
- [15] T.J. Moran, J.M. Gallego, I.K. Schuller, *J. Appl. Phys.* 78 (1995) 1887.
- [16] V. Skumryev, S. Stoyanov, Y. Zhang, G. Hadjipanayis, D. Givord, J. Nogués, *Nature (London, U. K.)* 423 (6942) (2003) 850.
- [17] X.H. Chen, K.Q. Wang, P.H. Hor, Y.Y. Xue, C.W. Chu, *Phys. Rev. B* 72 (2005) 054436.
- [18] Y.K. Tang, Y. Sun, Z.H. Cheng, *Phys. Rev. B* 73 (2006) 174419.
- [19] S.K. Giri, S.M. Yusuf, M.D. Mukadam, T.K. Nath, *J. Appl. Phys.* 115 (2014) 093906.
- [20] W. Liu, L. Shi, S. Zhou, J. Zhao, Y. Li, Y. Guo, *J. Appl. Phys.* 116 (2014) 193901.
- [21] W. Kohn, L.J. Sham, *Phys. Rev.* 140 (1965) A1133.
- [22] G. Kresse, J. Furthmüller, *Phys. Rev. B* 54 (1996) 111169.
- [23] P.E. Blochl, *Phys. Rev. B* 50 (1994) 17953.
- [24] S.L. Dudarev, et al., *Phys. Rev. B* 57 (1998) 1505.
- [25] J.P. Perdew, et al., *Phys. Rev. Lett.* 77 (1996) 3865.
- [26] J. Rodrigues-Carvajal, FULLPROF. A Rietveld Refinement and Pattern Matching Analysis Program (Laboratoire Leon Brillouin, CEA-CNRS, France, 2000).
- [27] M.T. Anderson, K.B. Greenwood, G.A. Taylor, K.R. Poeppelmeier, *Prog. Solid State Chem.* vol. 22, 1993, pp. 197–233.
- [28] G. King, P.M. Woodward, *J. Mater. Chem.* 20 (2010) 5785.
- [29] D. Rubi, et al., *J. Phys. Condens. Matter* 17 (2005) 8037.
- [30] L. Balcells, J. Navarro, M. Bibes, A. Roig, B. Martínez, J. Fontcuberta, *Appl. Phys. Lett.* 78 (2001) 781–783.
- [31] S. Vasala, M. Karppinen, *Prog. Solid State Chem.* 43 (2015) 1–36.
- [32] A. Aguadero, J.A. Alonso, M.J. Martínez-Lope, M.T. Fernández-Díaz, *Solid State Sci.* 13 (2011) 13–18.
- [33] Y.M. Jana, S. Nandi, A.A. Biswas, H.C. Gupta, R. Upadhyay, C. Upadhyay, D. Samanta, *Phys. Status Solidi B* 259 (2022) 2100460.
- [34] D. Serrate, J.M. De Teresa, M.R. Ibarra, *J. Phys. Condens. Matter* 19 (2007) 023201.
- [35] M.M. Shiralkar, C. Hao, X. Dong, T. Guo, L. Zhang, M. Li, H. Wang, *Supplementary information in Nanoscale* 6 (2014) 4735.
- [36] W.K. Zhu, Chi-Ken Lu, W. Tong, J.M. Wang, H.D. Zhou, S.X. Zhang, *Phys. Rev. B* 91 (2015) 144408.
- [37] K. Manna, R. Sarkar, S. Fuchs, Y.A. Onyikienko, A.K. Bera, G. Aslan Cansever, S. Kamusella, A. Maljuk, C.G.F. Blum, L.T. Corredor, A.U.B. Wolter, S.M. Yusuf, M. Frontzek, L. Keller, M. Iakovleva, E. Vavilova, H.-J. Grafe, V. Kataev, H.-H. Klauss, D.S. Inosov, S. Wurmehl, B. Büchner, *Phys. Rev. B* 84 (2016) 144437.
- [38] S. Dong, K. Yamauchi, S. Yunoki, R. Yu, S. Liang, A. Moreo, J.-M. Liu, S. Picozzi, E. Dagotto, *Phys. Rev. Lett.* 103 (2009) 127201.
- [39] J. Mao, Y. Sui, X. Zhang, X. Wang, Y. Su, Z. Liu, Y. Wang, R. Zhu, Y. Wang, W. Liu, X. Liu, *Solid State Commun.* 151 (2011) 1982.
- [40] E. Arenholz, K. Liu, Z. Li, I.K. Schuller, *Appl. Phys. Lett.* 88 (2006) 072503.
- [41] H.W. Zheng, Y.F. Liu, W.Y. Zhang, S.J. Liu, H.R. Zhang, K.F. Wang, *J. Appl. Phys.* 107 (2010) 053901.
- [42] J. Tauc, R. Grigorovici, A. Vancu, *Optical properties and electronic structure of amorphous germanium*, *Phys. Status Solidi B* 15 (1966) 627–637.
- [43] M.Z.M. Halizan, Z. Mohamed, A.K. Yahya, *Mater. Res. Express* 7 (2020) 8.
- [44] J.A. Khan, J. Ahmad, *Mater. Res. Express* 6 (2019) 115906.
- [45] S.R. Mohapatra, B. Sahu, S. Raut, S.D. Kaushik, A.K. Singh, *AIP Conf. Proc.* 1665 (2015) 140032.
- [46] N. Pandit, A. Dubey, T.K. Joshi, A. Shukla, U. Rani, P.K. Kamlesh, R. Gupta, T. Kumar, K. Kaur, A.S. Verma, *Int. J. Mod. Phys. B* (2024) 2550059.
- [47] S. Kumari, U. Rani, M. Rani, R. Singh, P.K. Kamlesh, S. Kumari, T. Kumar, A. S. Verma, *Mod. Phys. Lett. B* (2024) 2450323.
- [48] N.E. Kirchner-Hall, et al., *Appl. Sci.* 11 (5) (2021) 2395.
- [49] M.K. Niranjana, et al., *Phys. Rev. B* 70 (18) (2004) 180406.
- [50] R.M. Martin, *Electronic Structure: Basic Theory and Practical Methods*, second ed., Cambridge University Press, 2020.
- [51] M. Rani, P.K. Kamlesh, S. Kumawat, Anuradha, U. Rani, G. Arora, A.S. Verma, *Phys. B Condens. Matter* 680 (2024) 415645.